A stress scale in full-field identification procedures: a diffuse stress gauge

Stéphane Roux [a,*], François Hild [b], Stéphane Pagano [c]

[a] *Unité Mixte de Recherche CNRS/Saint-Gobain, 39, quai Lucien Lefranc, 93303 Aubervilliers cedex, France*
[b] *LMT-Cachan, ENS Cachan/CNRS-UMR 8535/Université Paris 6, 61, avenue du Président Wilson, 94235 Cachan cedex, France*
[c] *LMGC, UMR-CNRS 5508, Université Montpellier II, Case courier 048, place Eugène Bataillon, 34095 Montpellier cedex 5, France*

Abstract

Identification techniques solely based on displacement field measurements lack a stress scale and thus require a complementary information to be provided to complete the problem definition. Such a complementary test is proposed in this study, which is itself an identification designed for an unbounded two dimensional domain subjected to a normal point force on its boundary. A complex potential formulation is used to obtain a simple closed-form solution for the Poisson's ratio and Lamé's shear modulus. In order to evaluate the performance and robustness of this identification technique, the sensitivity to noise and error in grid positioning is investigated numerically.
© 2005 Elsevier SAS. All rights reserved.

1. Introduction

In Solid Mechanics, full field measurement techniques are more and more popular; photomechanics (Berthaud et al., 1995; Rastogi, 2000) has now reached a stage where the measurement of a whole kinematic field is compared to numerical simulations. The way experiments are performed has started to shift from mostly homogeneous situations (e.g., tensile or compressive tests) to heterogeneous cases in which full field measurements are unavoidable to analyze the results. One way of analyzing the tests is to identify property fields such as elastic parameters.

Identification procedures are being developed to identify isotropic or anisotropic, homogenous or heterogeneous elastic properties. Among them, updating techniques based upon the constitutive equation error (Ladevèze, 1975; Kohn and Lowe, 1988) have been used in the analysis of vibrations (Ladevèze et al., 1994), the identification of defects (Bui and Constantinescu, 2000) or elastic and/or damage fields (Geymonat et al., 2002), the study of heterogeneous tests (e.g., Brazilian test (Calloch et al., 2002)), or damage under dynamic loading condition (Feissel, 2003). An alternative to the previous approach is, for instance, the so-called virtual field method that has been used in a variety of situations mainly dealing with anisotropic and homogeneous properties of composite materials (Grédiac, 1989; Grédiac et al., 1999; Grédiac, 2004). Most of them require more or less complete stress/load measurements. Another identification procedure is based upon the reciprocity gap (Bui, 1995) that can be used to determine a local elastic field or to detect cracks in an elastic medium (Andrieux et al., 1997). In many of these

---

* Corresponding author.
   E-mail addresses: stephane.roux@saint-gobain.com (S. Roux), francois.hild@lmt.ens-cachan.fr (F. Hild),
stephane.pagano@lmgc.univ-montp2.fr (S. Pagano).

identification techniques, a very detailed (i.e., redundant) information is needed since both displacement and stress vector on the boundary are required (e.g., in the reciprocity gap method). This condition can be relaxed in some other approaches (e.g., constitutive equation error (Geymonat et al., 2002) or virtual field method (Grédiac, 1989)) where only an integral condition (i.e., resultant forces or moments) is needed.

Recently the extreme opposite philosophy has been advocated for, proposing to determine heterogeneous elastic/damage (Claire et al., 2002) (or thermal (Claire et al., 2003)) properties by using only displacement (or temperature) measurements with the so-called reciprocity gap method (Claire et al., 2004). Since no scale for stress or flux is fixed from the used data, only relative properties can be measured, and a global (uniform) scale factor for the elastic moduli or (thermal) conductivities remains undetermined. This approach has mainly been applied to identify damage fields, and variants exist for more complex field determination (e.g., independent Lamé coefficients (Claire, 2002)). To circumvent this difficulty at low cost, it is proposed to add just one static measurement to the kinematic ones (e.g., displacement field). The proposed scheme is to apply on the side of the specimen to be analyzed a point load with a known normal concentrated force F.

Let us mention that the inverse problem of stress identification underneath a contact has been addressed in the past based on surface displacements outside the contact zone (Ben Abdallah, 2000). This study is quite different in terms of problem setting and objectives. An axisymmetric distributed load was considered, a so-called Hertz–Mindlin contact problem (with a frictional interface), and the contact stresses were looked for based on known free surface displacements. One will rather consider a two dimensional (plane stress) geometry, where displacements are assumed to be known on a sectional plane. The identification of elastic constants is searched for rather than the detail of the contact stress. The issue of a finite contact zone and the role of distributed contact stresses rather than a point force are discussed below.

After introducing the problem in Section 2, some basic properties of 2D Kolossoff–Muskhelichvili potentials (Subsection 2.1) and Flamant's elementary solution (Subsection 2.2) are recalled. The solution is presented in Section 3. The relevance of a Flamant's solution in real cases is discussed in Section 4. To probe the sensitivity of the proposed tool to noise, the identification procedure is carried out on data that are artificially corrupted by a Gaussian noise. The effect of grid positioning with respect to the applied load is investigated. These analyses are presented in Section 5 in addition to some practical considerations concerning the scale at which the displacement measurements have to be performed and the performances of the measurement technique needed for the identification procedure. A summary of the main result, and a discussion underlining the use of such an approach is proposed in Section 6.

2. Problem definition

The following identification procedure is based on the analysis of a two-dimensional information, typically a surface displacement field obtained from digital image correlation. Therefore the following approach is restricted to either plane stress or plane strain. As shown schematically in Fig. 1, a point load is applied normal to the free surface of the sample. In the case of plates, which are suited to this approach, this requires the (2D) point load as being applied through the entire thickness of the sample. A straight boundary should also be present (a constraint that appears as tolerable). This restriction to plane elasticity is fundamental to the present study, however a vast literature shows that this hypothesis may be met in practical cases. Specific difficulties arising from this plane elasticity setting, and the use of a concentrated force in this context are discussed below.
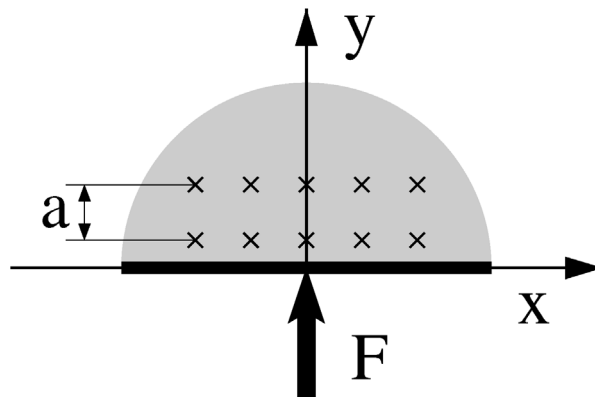

Fig. 1. A point force F is applied normal to the boundary (thick black line) of a solid (shown in gray). The measurement of the displacement at discrete points (shown as crosses distributed on a square grid of mesh size a), together with the value of the force are the input data allowing for the determination of the elastic constants.

Displacements are assumed to be measured at different points, for instance distributed over a regular grid with a characteristic mesh size a.

Locally, one knows the elastic problem in two dimensions, as Flamant's problem. Thus the knowledge of the displacement field close to the force at discrete points (in practice from ten to a few hundred points) can be used to estimate the Poisson's ratio and the shear modulus. The strategy is straightforward from now on. Mathematically, the convenient potential formulation of 2D elasticity is followed, although other routes may have been pursued (and would be required if the surface measurement were not representative of the depth, i.e., 3D problems).

2.1. Kolossoff–Muskhelichvili potentials

Let us use a local coordinate system with the origin at the point where the load is applied (see Fig. 1). Moreover, the 2D domain will be represented by complex numbers $z = x + iy$ (or using the polar form $z = r\,e^{i\theta}$), and the indented solid is supposed to lie in the $\Im(z) > 0$ half plane close to the origin. The Kolossoff–Muskhelichvili representation of the elastic problem in the complex plane is now briefly recalled. The potentials $\varphi(z)$ and $\psi(z)$ are two holomorphic functions (i.e., $\partial\varphi/\partial\bar{z} = \partial\psi/\partial\bar{z} = 0$), which allows one to retrieve the complex displacement field $\mathbf{U} = u_x + iu_y$ as (Muskhelishvili, 1933)

$$2\mu\mathbf{U} = \kappa\varphi(z) - z\overline{\varphi'(z)} - \overline{\psi(z)} \tag{1}$$

where μ is the Lamé's shear modulus, κ a dimensionless elastic coefficient that is related to the Poisson's ratio ν according to $\kappa = (3 - 4\nu)$ for plane strain, and $\kappa = (3 - \nu)/(1 + \nu)$ for plane stress conditions. The above displacement is determined up to a rigid body motion (which in complex notations reads $\mathbf{U}_0 + i\Omega z$ with Ω real).

The stress is conveniently represented through two combinations, first the (real) trace $S_0 = \sigma_{xx} + \sigma_{yy}$, and second the complex function $\mathbf{S} = \sigma_{yy} - \sigma_{xx} + 2i\sigma_{xy}$. From the potentials, they are written as

$$\begin{cases} S_0 = 2[\varphi'(z) + \overline{\varphi'(z)}], \\ \mathbf{S} = 2[\bar{z}\varphi''(z) + \psi'(z)]. \end{cases} \tag{2}$$

The Airy potential $\mathbf{A}$ can be expressed from these potentials as

$$\mathbf{A} = \Re[\bar{z}\varphi(z) + \Psi(z)] \tag{3}$$

with $\Psi'(z) = \psi(z)$.

2.2. Flamant's problem

The normal force indentation of an elastic domain has been solved by Flamant (Timoshenko and Goodier, 1970; Johnson, 1985). Embedded in the above notations, one can write

$$\varphi(z) = \psi(z) = \frac{iF}{2\pi}\log(z). \tag{4}$$

The displacement field becomes

$$\begin{aligned}
\mathbf{U} &= \frac{iF}{4\mu\pi}\left[\kappa\log(z) + \frac{z}{\bar{z}} + \log(\bar{z}) - (\kappa - 1)\frac{i\pi}{2} + 1 - (\kappa + 1)\log(r_0)\right] \\
&= \frac{iF}{4\mu\pi}\left[(\kappa + 1)\log(r/r_0) + (\cos(2\theta) + 1) - i(\kappa - 1)\left(\frac{\pi}{2} - \theta\right) + i\sin(2\theta)\right]
\end{aligned} \tag{5}$$

where a rigid displacement has been introduced in order to set $\mathbf{U}(z = ir_0) = \mathbf{0}$ at a conventionally chosen reference point located at a distance r_0 beneath the surface along the indentation axis.

3. Stress gauging

Let us now assume that the displacement is known at a number of discrete points z_n with $n = 1, \ldots, N$ inside the solid but close to the indentation point. These measured displacements are denoted by $\mathbf{U}_n$. In the absence of noise or deviation from the present hypothesis, for each point n, the following complex identity can be written

$$\kappa\left[\log(z_n) - \frac{i\pi}{2} - \log(r_0)\right] + (4i\mu\pi/F)\mathbf{U}_n = -\log(\bar{z}_n) - \frac{z_n}{\bar{z}_n} - \frac{i\pi}{2} - 1 + \log(r_0). \tag{6}$$

At this stage, it is important to remove the arbitrary rigid body motion that affects the experimental determination of $\mathbf{U}$. To achieve this aim, the above equation is averaged over all measurement points

$$\kappa\left[\langle\log(z)\rangle - \frac{i\pi}{2} - \log(r_0)\right] + (4i\mu\pi/F)\langle\mathbf{U}\rangle = -\overline{\langle\log(z)\rangle} - \left\langle\frac{z}{\bar{z}}\right\rangle - \frac{i\pi}{2} - 1 + \log(r_0) \tag{7}$$

where $\langle\cdot\rangle$ is the average operator. By subtracting both equations, the mean translation no longer appears

$$\kappa\left[\log(z_n) - \langle\log(z)\rangle\right] + (4i\mu\pi/F)\left(\mathbf{U}_n - \langle\mathbf{U}\rangle\right) = -\overline{\log(z_n)} + \overline{\langle\log(z)\rangle} - \frac{z_n}{\bar{z}_n} + \left\langle\frac{z}{\bar{z}}\right\rangle. \tag{8}$$

If the displacements are determined over a set of points that is symmetric with respect to the load axis, a rigid body rotation is easily removed by considering only the symmetric part of the displacement field with respect to the indentation axis, namely for all points z_n, $\mathbf{U}(z_n)$ is replaced by $(1/2)[\mathbf{U}(z_n) - \overline{\mathbf{U}}(-\overline{z_n})]$. If the data points are not symmetric with respect to the indentation axis, one can still use the same principle by adding the fictitious displacements $-\overline{\mathbf{U}}_n$ at points $-\overline{z_n}$. Here again, the mean rotation cancels out.

3.1. Solution

Let us introduce the following additional notations

$$\begin{cases} A_n = \log(z_n) - \langle\log(z)\rangle, \\ B_n = 4i\pi\left(\mathbf{U}_n - \langle\mathbf{U}\rangle\right)/F, \\ C_n = \overline{\log(z_n)} - \overline{\langle\log(z)\rangle} + z_n/\bar{z}_n - \langle z/\bar{z}\rangle \end{cases} \tag{9}$$

so that the identification procedure can be seen as minimizing the quadratic objective function $\mathcal{T}$

$$\mathcal{T}[\kappa, \mu] \equiv \sum_n |A_n\kappa + B_n\mu + C_n|^2 \tag{10}$$

with respect to κ and μ. In matrix form, one has to solve a linear system

$$[\mathbf{M}](\boldsymbol{\xi}) + (\boldsymbol{\chi}) = 0 \tag{11}$$

with

$$[\mathbf{M}] = \sum_n \begin{bmatrix} |A_n|^2 & \Re[A_n\overline{B}_n], \\ \Re[A_n\overline{B}_n] & |B_n|^2 \end{bmatrix}, \quad (\boldsymbol{\xi}) = \begin{pmatrix} \kappa \\ \mu \end{pmatrix}, \quad (\boldsymbol{\chi}) = \sum_n \begin{pmatrix} \Re[A_n\overline{C}_n] \\ \Re[B_n\overline{C}_n] \end{pmatrix}. \tag{12}$$

It is worth noting that the problem naturally gives rise to a quadratic function in κ and μ. It is not a specific feature coming from the potential formulation used herein, but rather a property of plane elasticity. Let us also note that, from dimensional analysis, only μ depends (linearly) with F. Thus the Poisson's ratio or equivalently the κ parameter can be determined without resorting to the force value.

Alternatively, one may also form the three *real-valued* vectors of length $2N$, α, β and γ, such that $\alpha_{2n-1} = \Re[A_n]$ and $\alpha_{2n} = \Im[A_n]$ (and similarly for β and γ with respectively B and C). Simple algebraic manipulations show that

$$[\mathbf{M}] = \begin{bmatrix} |\alpha|^2 & \alpha \cdot \beta \\ \alpha \cdot \beta & |\beta|^2 \end{bmatrix}, \quad (\boldsymbol{\chi}) = \begin{pmatrix} \alpha \cdot \gamma \\ \beta \cdot \gamma \end{pmatrix}. \tag{13}$$

In practice, it is highly unlikely that the vectors α and β are collinear so that the matrix $[\mathbf{M}]$ is invertible. Consequently, the κ coefficient can be expressed explicitly as

$$\kappa = \frac{|\beta|^2(\alpha \cdot \gamma) - (\alpha \cdot \beta)(\beta \cdot \gamma)}{|\alpha|^2|\beta|^2 - (\alpha \cdot \beta)^2} \tag{14}$$

independently of F since both numerator and denominator are homogeneous of degree 2 in β. The shear modulus is written as

$$\mu = \frac{|\alpha|^2(\beta \cdot \gamma) - (\alpha \cdot \beta)(\alpha \cdot \gamma)}{|\alpha|^2|\beta|^2 - (\alpha \cdot \beta)^2}. \tag{15}$$

This completes the procedure to be used.

4. Deviations from Flamant's solution

A point force in two dimensions (corresponding to a line in three dimensions) is a mathematical abstraction that cannot be encountered in practice close to the contact force. A distributed load over a small surface, e.g., Hertz contact (Johnson, 1985), is a more realistic case. Saint-Venant principle may however be invoked to restore some credibility to the present approach. More quantitatively, a distributed load over some finite surface of width δ will give rise to a displacement field that may be expanded over multipoles of increasing order. The dominant term will correspond to Flamant's problem (i.e., stress and strain decaying as $1/r$). The second term, because of $x \leftrightarrow -x$ symmetry, is not a dipole but rather a quadrupole (i.e., stress and strain decaying as $1/r^3$). Higher order terms will decay with distance with larger powers of r, $r^{-(2n+1)}$ with $n \geqslant 2$. The ratio of the first correction to the dominant term at a distance r from the center of the contact zone will be of order δ^2/r^2 as dictated by homogeneity.

In order to estimate the impact of such deviations, displacements are assumed to be known over a regular grid of points with a spacing a as shown in Fig. 1. For a contact zone which is as large as $a/10$, the closest point to the contact will be corrupted by a 1% change as compared to Flamant's solution. Further away, this correction will be quite negligible. Thus, since the goal is not to retrieve detailed information on the contact stresses (as for instance in (Ben Abdallah, 2000)), but rather to extract information on the elastic properties, one may safely resort to a point-like force as soon as the contact zone is sufficiently small as compared to the grid size. In a forthcoming section, the influence of the mispositioning of the grid as compared to the point of loading will be investigated. The difference between the actual and assumed displacement field is a dipole field, and hence a more severe discrepancy than the finite extent of a contact zone. Yet the procedure of symmetrizing the problem before estimating the elastic constants cancels out exactly this dipolar field, and thus only a quadrupolar correction is left. Therefore, in some sense, the sensitivity to error positioning is a good indication of the effect of a finite contact zone. We defer to that section for a more complete discussion on the quantitative aspects.

In the case of an elasto-plastic material where yielding occurs, the same argument holds, where δ is the extent of the plastic zone (i.e., of order F/σ_y if σ_y is the yield stress). Thus, as simple rule of thumb, the contribution of the plastic zone to the local displacement relative to the total displacement will be of order $(\sigma/\sigma_Y)^2$, i.e., the square of the local elastic stress relative to the yield stress.

One additional interest of the proposed procedure, because of the large redundancy of the (assumed) available information, is that one can trace back the contribution of each single measurement point to the error. For the above cases, where deviation from the ideal Flamant's problem is confined to the vicinity of the loading point, one can easily detect that the loading zone creates deviation from the identified displacement field. Once a physical reason for such a deviation is identified or hypothesized, the same computation can be performed excluding measurement points where non-linear, or non punctual contact is suspected because of increasing local error. Alternatively, the basis of displacement field can be enriched with a quadrupolar term.

5. A (numerical) test case

5.1. Noise sensitivity

The displacement field is computed numerically from the above formula at N_{pt} discrete points. The latter are distributed over a regular mesh $(i_x a; (i_y + 1/2)a)$ with $-n \leqslant i_x \leqslant n$ and $0 \leqslant i_y \leqslant n - 1$, so that $N_{pt} = n(2n+1)$. In the following two examples are chosen, namely, $n = 2$ and $n = 10$ (with $N_{pt} = 10$ and $N_{pt} = 210$, respectively). Numerically, the following values $a = 1$, $F/(4\pi\mu_{\text{true}}a) = 1$ and $\nu_{\text{true}} = 0.25$ are used under plane stress conditions. The displacement field data is then "corrupted" by the addition of a random noise (with no spatial correlation). The latter is characterized by a Gaussian distribution of zero mean and standard deviation ϵ. The level of ϵ is to be compared to the average amplitude $\langle|\mathbf{U}|\rangle$ of the displacements, which depends on the chosen grid, namely, $\langle|\mathbf{U}|\rangle/a = 7.3$ for $N_{pt} = 210$, and $\langle|\mathbf{U}|\rangle/a = 3.0$ for $N_{pt} = 10$ (Fig. 1).

For 10000 different samplings of the noise, the Poisson's ratio ν_{est} and shear modulus μ_{est} (scaled by the force and mesh size of the grid) are estimated. They are subsequently rescaled by their initially chosen value, so that the method accuracy can be determined. The dimensionless indicators are thus $Z_\nu = \nu_{\text{est}}/\nu_{\text{true}}$ and $Z_\mu = \mu_{\text{est}}/\mu_{\text{true}}$. These simulations provide both the systematic error through the average value of Z, and the uncertainty σ_ν and σ_μ as the standard deviation of the corresponding Z.

Table 1 and Fig. 2 give the average Z ratio for the two grids and different noise amplitudes. For a vanishing noise, the results are as expected $Z_\nu = Z_\mu = 1$. As noise is increased, the Poisson's ratio becomes systematically overestimated while the shear modulus is underestimated. The measurement error $|Z - 1|$ increases quadratically with the noise amplitude. This quadratic dependence can be explained by using a small perturbation approach exploiting the expression of κ and μ Taylor expanded in β. Because the noise has a zero average, the first systematic deviation from the mean value comes from quadratic terms in the noise. The influence of the number of data points and their distribution in the horizontal and vertical directions is rather weak,

Table 1
Systematic error Z and uncertainty σ on the determination of the Poisson's ratio ν and the Lamé's shear modulus μ. Two numbers of data points N_{pt}, and different noise amplitudes ϵ are considered

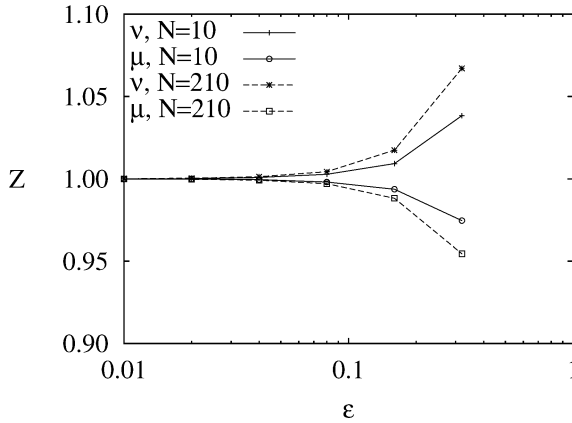| ϵ	$N_{pt} = 10$				$N_{pt} = 210$			
	Z_ν	σ_ν	Z_μ	σ_μ	Z_ν	σ_ν	Z_μ	σ_μ
0.01	1.0000	0.0049	0.9999	0.0020	1.0001	0.0011	0.9999	0.0005
0.02	1.0001	0.0097	0.9999	0.0040	1.0003	0.0022	0.9998	0.0010
0.04	1.0004	0.0196	0.9996	0.0081	1.0011	0.0044	0.9992	0.0019
0.08	1.0022	0.0388	0.9981	0.0162	1.0045	0.0087	0.9971	0.0038
0.16	1.0101	0.0787	0.9937	0.0325	1.0174	0.0172	0.9882	0.0074
0.32	1.0351	0.1524	0.9746	0.0621	1.0669	0.0328	0.9545	0.0138

Fig. 2. Ratio of estimated versus real elastic constants, for the Poisson's ratio ν (top curves), and shear modulus μ (lower curves). In the caption, N refers to the number N_{pt} of points used for the analysis.
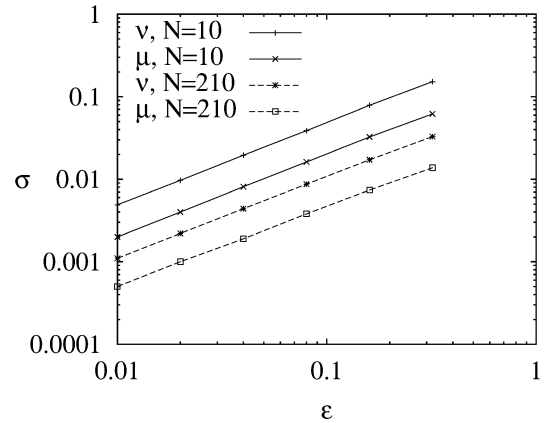

Fig. 3. Uncertainty on the determination of ν and μ for different numbers of points N_{pt} and noise levels ϵ.

and ironically, for a larger number of data points, the systematic error increases both for μ and ν. Presumably, only the close proximity of the point load is informative on the mechanical behavior, whereas remote points are more sensitive to noise.

More important, for the practical use of this tool, is the estimate of the uncertainties, σ_ν and σ_μ, displayed in Table 1 and Fig. 3. Both of them vary in proportion to ϵ as shown in Fig. 3 (data points aligned on straight lines of slope unity in a log–log plot). A more systematic study on the influence of the number of measurement points N_{pt} shows that σ decreases as $N_{pt}^{-1/2}$. This can be interpreted as the consequence of the central limit theorem. More precisely, a numerical fit to the data reads

$$\sigma_\nu \approx 1.55 \frac{\epsilon}{\sqrt{N_{pt}}}, \qquad \sigma_\mu \approx 0.66 \frac{\epsilon}{\sqrt{N_{pt}}}. \tag{16}$$

It can be noted that the uncertainty associated to the identified elastic parameters is directly proportional to ϵ that characterizes the (standard) uncertainties in terms of displacement measurement. This point will be further studied later.

5.2. Influence of errors in grid positioning

One possible source of error from the estimate of the displacements was considered above. However, the positioning of the grid itself may induce deviations from the expected solution. In order to test this possibility and quantify it, direct numerical simulations are performed, and an offset (Δ_x, Δ_y) is introduced in between the origin of the grid coordinates and the point of loading. This offset is then ignored in the analysis, and the induced error in μ and ν is evaluated.

Both coordinates do not play the same role. Because of the fact that the contact point is always in practice distributed over a finite surface, the Δ_x offset may be significant. Values of Δ_x as large as $a/10$ are considered, where a is the mesh size (Fig. 1). Conversely, the accuracy of the grid positioning in the y direction, normal to the boundary, is typically much less. For a smooth boundary, it is common to be able to resolve its position to a fraction of pixel. Since a is typically 16 or 32 pixels wide, Δ_y/a should be of the order of 1%. Yet, in the numerical study, ten times larger values are investigated.

The separate effects of Δ_x and Δ_y are shown in Figs. 4 and 5, respectively. The error is linear in Δ_y, but quadratic in Δ_x. This property results from an argument discussed in Section 4. An offset in y gives rise to a difference in displacement field
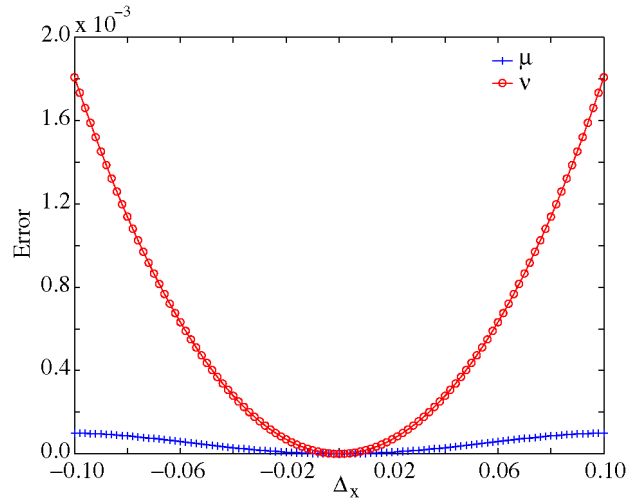
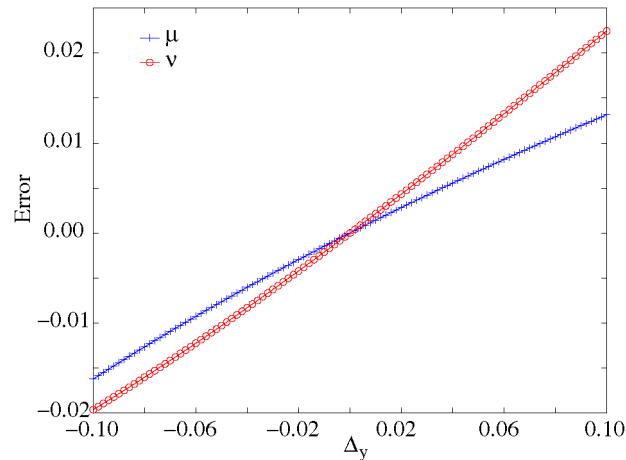Fig. 4. Error due to an offset in grid positioning parallel to the boundary.

Fig. 5. Error due to an offset in grid positioning normal to the boundary.

which is a dipole field, whereas the x offset, because of the symmetrization procedure ($x \leftrightarrow -x$ symmetry), gives rise to a quadrupole field. For the largest values of Δ_x/a (respectively Δ_y/a) considered (0.1), the maximum error reaches 0.2% (respectively 2%) on the most sensitive quantity ν. Following the argument on feasible accuracies in the location of the grid origin, errors should be strictly smaller than one percent.

As argued in Section 4, the error induced by an offset Δ_x can be compared to the effect of a contact taking place over a finite extent, as in Hertz contact. The radius of contact R will result in a smaller equivalent Δ_x, if one focuses only on the quadrupolar term (namely $\Delta_x = (\sqrt{\pi}/4)R \approx 0.44R$), so that the maximum error is reached for a radius of contact (relative to the grid size a) $R/a \approx 0.22$. Figs. 6 and 7 display maps of errors (absolute values) for joint errors in x and y. No drastic coupling effects occur, and looking for extreme values of error, 1.6% and 2.5% are obtained for the most severe cases respectively for μ and ν.

The conclusion of these two sub-sections is that experimental errors, be they uncertainty in the displacement evaluation or in the grid positioning, have a rather limited impact on the estimates of elastic properties, and hence the approach appears to be quite robust, although experimental tests have to be performed in order to secure this statement.

5.3. Applicability to an experimental example

In the following, it is assumed that DIC (i.e., digital image correlation (Périé et al., 2002)) is used to determine displacement fields. It consists in matching small zones, i.e., interrogation windows, in a reference image prior to applying a load and in a picture of the surface when the load is applied. Each measurement "point" corresponds to the center of an interrogation window
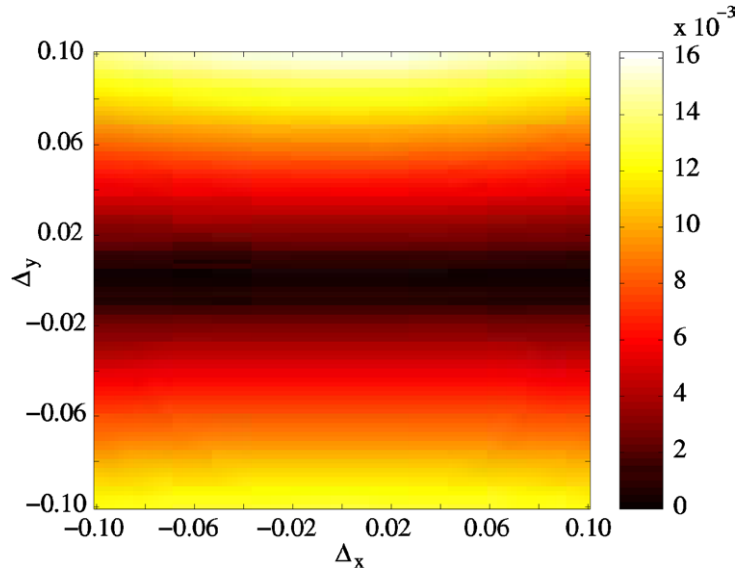
Fig. 6. Error on the determination of μ due to an offset parallel Δ_x and normal Δ_y to the boundary. Both of these offset distances are scaled by the grid mesh size.
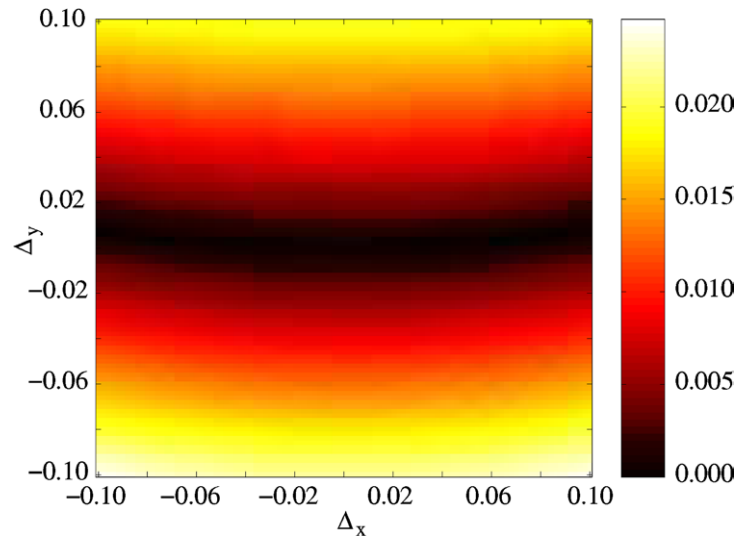

Fig. 7. Error on the determination of ν due to an offset parallel Δ_x and normal Δ_y to the boundary. Both of these offset distances are scaled by the grid mesh size.

of size $\delta \times \delta$ pixels. The separation between two interrogation windows is equal to a (Fig. 1). When using this type of technique with 8-bit pictures, a displacement resolution (Périé et al., 2002) and uncertainty (Bergonnier et al., 2005) ϵ of the order of 2×10^{-2} pixel can be achieved for an interrogation window of 16×16 pixels (i.e., $\delta = 16$ pixels), and 10^{-2} pixel when $\delta = 32$ pixels.

Let us consider an example of a steel (i.e., $\mu \approx 100$ GPa) plate of thickness $e = 10$ mm subjected to a load P equal to 1 kN. The condition that the displacement variation between two neighboring measurement points (separated by a distance a, Fig. 1) be greater than the displacement uncertainty defines the maximum distance $R_{\max}$ to the applied load for which significant data can be obtained

$$R_{\max} \propto \frac{P}{\pi \mu e} \frac{a}{\epsilon} \tag{17}$$

so that $R_{\max} \approx 0.25$ mm when $\delta = a = 16$ pixels, and $R_{\max} \approx 1$ mm when $\delta = a = 32$ pixels. Consequently, a long distance microscope should be used in both cases with a magnification such that 1 pixel corresponds to about 1 μm. When the applied load is multiplied tenfold, a conventional zoom can be used instead when the size δ of the interrogation window is equal to 32 pixels.

There exists also a lower limit $R_{\min}$ in terms of distance caused by yielding of the material

$$R_{\min} \propto \frac{P}{\pi \sigma_y e}. \tag{18}$$

In the previous situation with $\sigma_y \approx 100$ MPa, $R_{\min} \approx 0.3$ mm so that there is a large zone for which displacement measurements are relevant to the approach proposed herein when the size of the interrogation window is equal to 32 pixels. For a 16-pixel interrogation window, the uncertainty is too high to get relevant data. The following condition

$$\frac{\sigma_y}{\mu} > \frac{\epsilon}{a} \tag{19}$$

must be satisfied in order to perform an identification with displacements whose uncertainty is acceptable with respect to their level. The left hand side of the previous equation only depends upon material parameters, whereas the right hand side is related to the performance of the measurement technique in terms of (standard) strain uncertainty. It can be noted that this type of discussion allows the user to choose the correlation parameters, based upon conditions imposed by the identification procedure. When $r_0 = R_{\max}$, the mean displacement is such that $\langle |\mathbf{U}| \rangle \approx 0.34 R_{\max} \epsilon / a$, value that is 10 times greater than ϵ when the magnification is such that 1 pixel corresponds to 1 μm. Consequently the mean error in the identification of the elastic constants is expected to be less than 5 % when 10 measurement points are used (Fig. 2).

6. Discussion and conclusion

The proposed use of displacement measurements in the vicinity of a normal indentation point, in plane elasticity, provides a stress gauge as soon as the indentation force is known. This information can be used in any further analysis based solely on kinematic fields to identify elastic properties, stress intensity factors, or more complex situations (e.g., heterogeneous materials, non-linear behavior). Independence from other loading applied to a sample can be introduced by using Saint-Venant's principle. This is a natural trend that can be pushed to the extreme by cutting the sample into two parts, one for the elastic identification, and the other one for any other use in digital image correlation. The only advantage there is the homogeneity of the technique used. Furthermore, the results presented herein can be extended to deal with contact (e.g., Hertzian) problems that are often encountered experimentally (e.g., flexural tests, Brazilian test).

Let us point out that insisting for having decoupled problems might not be the optimal solution. On the contrary, the novel concept of "*diffuse stress gauging*" refers to the fact that the above procedure can be associated with other load patterns, so that the support of the stress gauge is diffuse on the sample face. Suppose that a complex load is applied to the sample, for instance to characterize a complex crack propagation problem. A point load can be superimposed and contribute to the displacement in a large part of the sample, and yet can be used in an identification procedure, associating both the main loading (with its full complexity) and an additional indentation. In practice, this means to stop the present analysis at Eq. (6), and add to the latter other contributions. All additional measurements can be purely kinematic. The system to invert will then be more complex than the simple (i.e., decoupled) 2×2 linear system in the present case. Still the addition of the point load will allow for this "stress gauging," and the term diffuse is proposed here to emphasize that in such case the main test and the stress gauging may share spatially a significant part of the domain.

Furthermore, one important point should be emphasized. A symmetrization procedure has been designed to eliminate the effect of rotations (and spurious dipolar corrections). Substraction of the average value of all determining equations has been proposed to avoid the dependence on the artificial rigid translation that has to be included in Flamant's solution (i.e., a pathology of the two dimensional case). This in turn implies an independence of the procedure with respect to any rigid body motion. Proceeding along the same lines, one may construct a set of equations that is orthogonal to an arbitrary constant strain over the region of interest. This will produce a system that is mathematically decoupled from any other loading that induces a constant strain over this region. Part of this decoupling is already present at this stage for symmetry reason, i.e., a simple shear strain ε_{xy} cannot couple to the system because of the $x \leftrightarrow -x$ symmetry.

Such a concept of "diffuse stress gauging" is, to the authors' knowledge, original. Yet, as the identification of elastic properties based on image analysis is a rapidly growing field, one may mention that the use of this concept allows one to relax the conditions usually considered to achieve well-posedness in identification problems. One single load measurement on the side of the sample has been shown here to be sufficient to capture the elastic properties of a (homogeneous part of a) solid. This is to be contrasted with the common practice that consists in using richer static data.

Let us finally note that due to the singular behavior of the displacement field close to the indentation point, standard DIC may not be the most appropriate tool. An integrated approach based on elastic displacement fields (including Flamant's field) using in the analysis of raw images can be performed following the general approach proposed by Wagne et al. (2002). The performance of the latter approach (yet to be developed) is expected to be much better, and thus the 1% accuracy is expected to be well within reach experimentally. A similar strategy has revealed extremely powerful for crack detection (Hild and Roux, 2005).

Acknowledgements

References

Andrieux, S., Abda, A.B., Bui, H.D., 1997. Sur l'identification de fissures planes via le concept d'écart à la réciprocité. C. R. Acad. Sci. Paris, Sér. I 324, 1431–1438;
See also, Andrieux, S., Abda, A.B., Bui, H.D., Reciprocity principle and crack identification. Inverse Problems 15 (1999) 59–65.

Ben Abdallah, J., Bonnet, M., 2000. Une approche non-destructive pour l'identification des contraintes de contact. C. R. Acad. Sci. Paris, Sér. IIb 328, 525–529.

Bergonnier, S., Hild, F., Roux, S., 2005. Strain heterogeneities in tension and compression tests on mineral wool samples. J. Strain Anal. 40 (2), 185–197.

Berthaud, Y., Paraskevas, D., Taroni, M. (Eds.), 1995. Photomécanique 95. GAMAC, Paris, France.

Bui, H.D., 1995. Sur quelques problèmes inverses élastiques en mécanique de l'endommagement. In: Proceedings 2e Colloque national de calcul des structures. Hermes, Paris, France, pp. 25–35.

Bui, H.D., Constantinescu, A., 2000. Spatial localization of the error of constitutive law for the identification of defects in elastic solids. Arch. Mech. 52, 511–522.

Calloch, S., Dureisseix, D., Hild, F., 2002. Identification de modèles de comportement de matériaux solides : utilisation d'essais et de calculs. Technologies et Formations 100, 36–41.

Claire, D., 2002. Identification de propriétés thermomécaniques résolues spatialement, MSc report, ENS Cachan.

Claire, D., Hild, F., Roux, S., 2002. Identification of damage fields using kinematic measurements. C. R. Mecanique 330, 729–734.

Claire, D., Hild, F., Roux, S., 2004. A finite element formulation to identify damage fields: The equilibrium gap method. Int. J. Numer. Methods Engrg. 61 (2), 189–208.

Claire, D., Roux, S., Hild, F., 2003. Identification de conductivités thermiques et de propriétés élastiques locales par analyse de champs. Méc. Ind. 4, 655–665.

Feissel, P., 2003. Vers une stratégie d'identification en dynamique rapide pour des données incertaines, PhD dissertation, ENS de Cachan.

Geymonat, G., Hild, F., Pagano, S., 2002. Identification of elastic parameters by displacement field measurement. C. R. Mecanique 330, 403–408.

Grédiac, M., Pierron, F., Surrel, Y., 1999. Novel procedure for complete in-plane composite characterization using a single T-shaped specimen. Exp. Mech. 39 (2), 142–149.

Grédiac, M., 1989. Principe des travaux virtuels et identification. C. R. Acad. Sci. Paris, Sér. II 309, 1–5.

Grédiac, M., 2004. The use of full-field measurement methods in composite material characterization: interest and limitations. Composites: Part A 35, 751–761.

Hild, F., Roux, S., 2005. Measuring ceramic toughness with a microscope, in preparation.

Johnson, K.L., 1985. Contact Mechanics. Cambridge University Press, Cambridge, UK.

Kohn, R.V., Lowe, B.D., 1988. A variational method for parameter identification. Math. Models Numer. Anal. 22 (1), 119–158.

Ladevèze, P., 1975. Comparaison de modèles de milieux continus, Thèse d'Etat, Université Paris 6;
See also P. Ladevèze, Updating of complex structure models, Technical report 33.11.01.4, Aérospatiale, les Mureaux, France, 1983.

Ladevèze, P., Nedjar, D., Reynier, M., 1994. Updating of finite element models using vibration tests. AIAA 32 (7), 1485–1491.

Muskhelishvili, N.I., 1933. Some basic problems of the mathematical theory of elasticity, Acad. Sci. USSR, Leningrad, USSR (in Russian).

Périé, J.N., Calloch, S., Cluzel, C., Hild, F., 2002. Analysis of a multiaxial test on a C/C composite by using digital image correlation and a damage model. Exp. Mech. 42 (3), 318–328.

Rastogi, P.K. (Ed.), 2000. Photomechanics, vol. 77. Springer, Berlin, Germany.

Timoshenko, S.P., Goodier, J.N., 1970. Theory of Elasticity, 3rd ed. McGraw-Hill, New York.

Wagne, B., Roux, S., Hild, F., 2002. Spectral approach to displacement evaluation from image analysis. Eur. Phys. J. AP 17, 247–252.